crystals

MDPI

Article

Influence of Deposition Time on Structural, Morphological, and Optical Properties of CdS Thin Films Grown by Low-Cost Chemical Bath Deposition

Abdelhamid El-Shaer [1,*], Sameh Ezzat [2], Mohamed A. Habib [3,4,*], Omar K. Alduaij [3], Talaat M. Meaz [2] and Samy A. El-Attar [2]

[1] Physics Department, Faculty of Science, Kafrelsheikh University, Kafrelsheikh 33516, Egypt
[2] Physics Department, Faculty of Science, Tanta University, Tanta 31527, Egypt; talaatmewz@yahoo.com (T.M.M.)
[3] Chemistry Department, College of Science, Imam Mohammad Ibn Saud Islamic University (IMSIU), Riyadh 11623, Saudi Arabia; okduaij@imamu.edu.sa
[4] Chemistry of Tanning Materials and Leather Technology Department, Chemical Industries Institutes, National Research Center, Dokki, Giza P.O. Box 12622, Egypt
* Correspondence: elshaer@sci.kfs.edu.eg (A.E-S.); mahabib@imamu.edu.sa (M.A.H.)

Abstract: CdS thin films were deposited on glass substrates employing low-cost and low-temperature chemical bath deposition (CBD). The effect of deposition time on the fabricated sample's properties was investigated by XRD, SEM, EDX, Raman, UV-vis spectrophotometry, and PL spectroscopy. XRD results indicate the formation of cubic and hexagonal structures of CdS thin films. The calculated average crystal size ranged from 21–50 nm. SEM results indicate the formation of hierarchical nanoflakes where the nanoflakes are entangled with one another like plant roots. Raman study confirmed that the fabricated thin films have two distinct peaks that are centered at 298 cm^{-1} and 599 cm^{-1}, which are characteristic vibration modes for CdS thin film. UV-vis absorption spectra indicate absorption band edges near 500 nm, which are related to the band gap values of CdS thin films. The estimated Eg of CdS thin films was reduced from 2.4 to 2.22 eV as the deposition time increased from 5 to 60 min. PL results show the main peak centered at 537 nm, its intensity decreasing as deposition time increases, indicating lower recombination of charge carriers. Our results reveal that CdS thin films are an excellent candidate for optoelectronic applications.

Keywords: CdS; thin films; low-cost; CBD technique; optical studies; optoelectronic applications

Citation: El-Shaer, A.; Ezzat, S.; Habib, M.A.; Alduaij, O.K.; Meaz, T.M.; El-Attar, S.A. Influence of Deposition Time on Structural, Morphological, and Optical Properties of CdS Thin Films Grown by Low-Cost Chemical Bath Deposition. *Crystals* **2023**, *13*, 788. https://doi.org/10.3390/cryst13050788

Academic Editor: Stefano Carli

Received: 3 April 2023
Revised: 4 May 2023
Accepted: 6 May 2023
Published: 9 May 2023

1. Introduction

Cadmium sulfide (CdS) is an n-type semiconductor that is suitable for use in solar cells fabricated from chalcogenide materials such as Cu(In, Ga)Se_2, CdTe, Cu_2ZnSnS_4, and PbS [1–7]. It has a wide band gap energy of about 2.42 eV with a high absorption coefficient and high mobility. CdS also has significant potential in many applications, such as photosensors and thin-film transistors [8,9]. There are many different techniques to deposit CdS, such as chemical bath deposition (CBD) [5,10–13], vaporization [14], spray pyrolysis [15], sputtering [16], and successive ionic layer adsorption and reaction [17]. However, CBD as a low-cost and low-temperature technique could produce CdS thin films with high uniformity and large-scale area. In general, CBD is a direct and cheap method that enables the deposition of several chalcogenides including CdSe, ZnO, Sb_2Se, Bi_2Se, ZnS, and CuS where many parameters such as pH, precursor concentrations, and bath temperature could be employed to have different material shapes and properties [18–23]. Recently, many papers were published on different properties and features of bulk CdS grown using CBD [13–18]. Some of these publications have tried to explain the primary stages of the nucleation and development of CdS thin films. D.A. Mazón Montijo et al.

determined that the growth and nucleation of CdS thin films depended on the earliest nucleation centers of $Cd(OH)_2$ [24]. A. Oliva et al. examined the early steps of deposition CdS thin films on different substrates including indium tin oxide (ITO), glass, and silicon (Si) substrates. Depth shapes obtained from Auger electron spectroscopy were used to demonstrate how the shape and microstructure changed in polycrystalline thin films where the CdS/substrate boundary played an important role in the growth rate [25]. N. S. Kozhevnikova et al. surveyed the principal creation of nanocrystalline CdS thin films using X-ray grazing incidence diffraction. The manufacture of an adhesive CdS thin film, according to the authors, is dependent on the development of a cadmium hydroxide barrier layer between CdS thin film and Si substrate [26]. pH value plays an important role in chemical bath deposition [27,28], and therefore a few articles have discussed the starting pH and how it changes during the reaction procedure, which could have an influence on the mechanism for thin film development [29,30].

Moreover, deposition time influences the physical properties of the fabricated thin films; therefore, a few papers were published to investigate the effect of deposition time on the properties of CdS films. Moualkia et al. [31] used different deposition times to produce CdS thin films and found that, with increasing time, the formed CdS films changed from cubic structure to a mix of orthorhombic and cubic structure. They also indicated that the crystallite sizes increased with rising deposition time. Barote et al. [32] examined the impact of deposition time on thicknesses of CdS thin films and found that the layer's thicknesses are heightened and then decreased subsequently. There are many CdS growth mechanisms suggested for the variation of deposition time. Sandoval-Paz et al. used spectroscopic ellipsometry to determine the growth kinetics for CdS films produced from an ammonia-free CBD process [33]. They indicated that with shorter times, ion−by−ion produces dense inner layer. With longer times, the outer layer develops; in such cases, lower precursor concentrations result from a slower growth rate where cluster−by−cluster growth takes place [33]. A. S. Najm et al. studied the mechanism for the combined growth of CdS films that electrostatically bonded to soda-lime glass, producing intermediate complexes $[Cd(NH_3)_4]^{2+}$ that assisted in the collision of such complexes with a soda-lime glass slide [34]. Moreover, almost all the published studies used complex agents to produce CdS thin films. Therefore, here we present the impact of deposition time on structural, morphological, and optical properties of CdS thin films grown on normal glass substrates employing low-cost chemical bath deposition (CBD) without a complexing agent or annealing temperature. The fabricated thin films are characterized by employing different techniques, especially Raman and PL spectroscopy, to investigate the recombination, separation, and collection of charge carriers as a step to evaluate CdS thin films for optoelectronic applications.

2. Materials and Methods

2.1. Materials

Potassium hydroxide [KOH, purity 99.5%, Aldrich], Thiourea [H_2NCSNH_2, purity 99%, Aldrich)], cadmium sulfate [$3CdSO_4.8H_2O$, purity 99%, Oxford, UK], deionized water (DIW) (Milli-Q, 18 MΩ·cm), and Corning glass used as a substrate.

2.2. Sample Synthesis

The glass substrates were cut to 2 cm × 2.5 cm for deposition of CdS thin films. To clean the substrates, a detergent solution was used where substrates were rinsed with DIW and then sonicated for 15 min in isopropyl alcohol, acetone, and DIW, followed by drying at 120 °C. A low-cost and low-temperature CBD technique was employed to fabricate CdS thin films on glass substrates. For this, 20 mL of DIW was used to dissolve 0.08 M of (3 $CdSO_4.8H_2O$) and 0.2 M of Thiourea in which the two solutions were separately dissolved, as shown in Figure 1. The resulting mixture was agitated for 10 min, adjusted to a pH of 10.5, and then placed in an 80 °C water bath for 30 min.

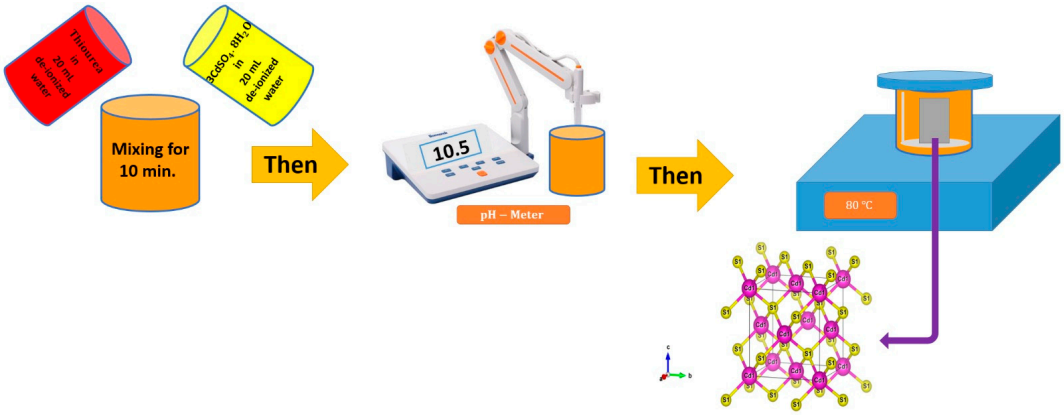

Figure 1. Schematic diagram of CBD technique for growing CdS thin films.

Similar steps were taken to produce CdS nanostructures where the deposition time varied from 5 to 60 min. The bath was entirely covered throughout the deposition. The resulting substrate was repeatedly washed with DIW. It was then subjected to a 4 h drying process at 80 °C in a hot-air oven before further characterization.

The fabricated samples were uniform, transparent, sticky, and yellow, as presented in Figure 2. The XRD (Shimadzu 6000) was used to measure the thin-film structure with two thetas ranging from 10 to 70. The morphology properties of the fabricated thin films were examined using scanning electron microscopy (SEM) [JSM-651OLV]. A spectrophotometer (JASCO V-630) and a photoluminescence (PL) equipment outfitted with an iHR320 spectrometer were used to evaluate optical characteristics (HORIBA). Raman spectra were collected through Raman spectroscopy using a WITec alpha300 R (WITec Wissenschaftliche Instruments, Ulm, Germany).

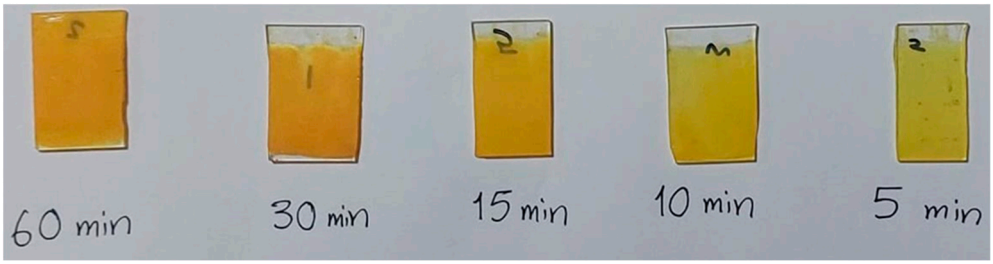

Figure 2. Photographic pictures of the fabricated samples at different growth time as written (5, 10, 15, 30, and 60 min).

3. Results and Discussion

3.1. Analysis of Structural Properties

X-ray diffraction patterns of the CdS thin films at various deposition times are shown in Figure 3. The peak at 26.60° which corresponds to the (111) plane has the highest intensity, confirming the formation of CdS thin films on the cubic structure (JCPDS # 36-1451 card) [1]. However, the peaks associated with planes (110) and (112) at about 44.4° and 52.0°, respectively, specified that a mixture of hexagonal and cubic phases was formed [2]. The strength of peaks varies with the deposition time, increasing to 10 min and then decreasing. This suggests that the ideal deposition time for maximizing crystallinity is 10 min, as deposition time has a significant impact on the crystallization of the film [3]. Depending on the manufacturing technique, CdS could have either a more stable hexagonal or cubic sphalerite crystal structure [7]. Moreover, Figure 3 shows that the glass substrate is the reason for the enormous hump in the entire set of X-ray diffraction diagrams at the peak at 26.7° [8]. Rietveld refinements of XRD data are attached as a supplementary file.

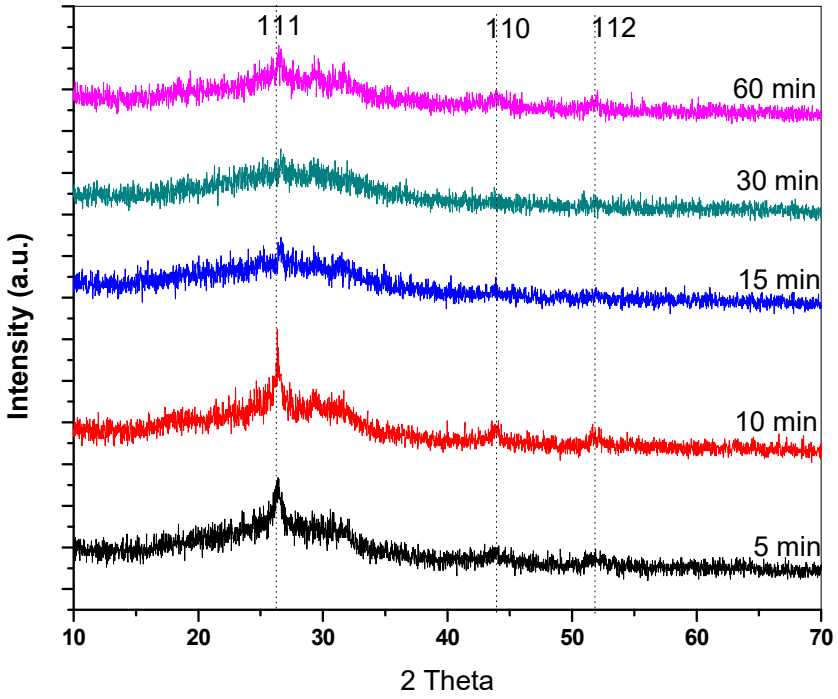

Figure 3. XRD patterns of fabricated CdS thin films with various deposition times.

Lattice parameters were calculated using XRD data as follows [1]:

$$a = d_{hkl}\sqrt{h^2 + k^2 + l^2} \quad (1)$$

Employing the Scherrer equation, the average crystal sizes (D) for the CdS thin films could be calculated [2]:

$$D = \frac{0.9\lambda}{\beta \cos\theta} \quad (2)$$

where λ is the X-ray wavelength (λ = 0.1544 nm), β is the full width at half maximum (FWHM), and θ is the Bragg angle of the related peak.

The following equation determines the density of dislocation of thin films:

$$\delta = \frac{1}{D^2} \quad (3)$$

and the microstrain (ε) of thin films could be estimated [3]:

$$\varepsilon = \frac{\beta \cot\theta}{4} \quad (4)$$

Table 1 presents the calculated D, δ, ε, and band gap values, from which it is clear that the crystal size decreases from about 20 nm to about 15 nm with increasing deposition time and then increases with further deposition time, as shown in Figure 4. This could be attributed to the number of Cd^{2+} ions, which decreases with time, and this gives time for particles to enlarge. In such cases, the vertical growth becomes the major portion which produces smaller crystal size with increasing deposition time. With further increasing deposition time, the lateral growth becomes higher than vertical growth, producing a bigger crystal size. Moreover, strain increases with the raising of deposition time, which indicates increasing particle size.

Table 1. The calculated D, δ, ε, and band gap values from the XRD and UV-VIS data of CdS thin films.

Deposition Time (min)	FWHM	2 θ (111)	d_{hkl} (Å)	a (Å)	D (nm)	$\delta \times 10^{14}$ Lines/m^2	$\varepsilon \times 10^{-3}$	Band Gap (eV)
5	0.39	26.37	3.38	5.85	21.08	0.002251	3.40	2.40
10	0.55	26.39	3.38	5.84	14.97	0.004465	4.79	2.32
15	0.47	26.36	3.34	5.79	17.50	0.003264	4.10	2.25
30	0.22	26.66	3.34	5.79	36.60	0.000747	1.93	2.23
60	0.16	26.38	3.38	5.85	50.98	0.000385	1.41	2.21

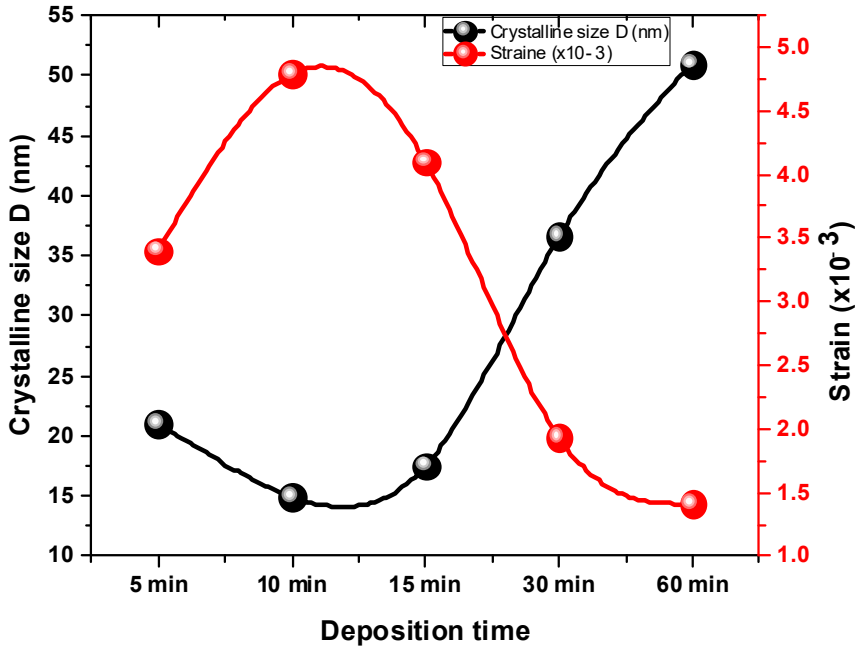

Figure 4. Correlation between the crystallite size and strain as a function of deposition time.

3.2. SEM Analysis

Analysis of the morphology for the fabrication of CdS thin films was carried out using SEM. Figure 5 displays top-view SEM images of CdS thin films with different deposition times of 5, 10, 15, 30, and 60 min. All samples resemble hierarchical nanoflakes. The nanoflakes are entangled with one another like plant roots. In every location, the samples were discovered to be uniformly homogenous and smooth, demonstrating that the deposited film was uniformly yellowish, adhering and completely coated to the substrate with no pinholes or cracks in any of the coatings. The minuscule particles are joined together in a porous structure that resembles fibrous material, indicating the created CdS thin films are nanocrystalline. Moreover, thin films are covered in spherical granules, and as deposition times increase, the density of particles rises. A homogenous layer is created when the microscopic particles continue to collect and cover the entire substrate surface. Little particles condense into bigger clusters that are evenly dispersed throughout the films as the deposition time is extended to 60 min. Such morphology could be explained by the increase in deposition time, the shape of coral reefs, and cross-linked increases where more precursor ions decrease and both lateral and vertical growth increase. Therefore, more particles were agglomerated to each other, forming lines of string beans [35]. Such results could also be explained by shorter times where ion-by-ion growth takes place, producing less particle size, while with longer times, lower precursor concentrations result from a slower growth rate where cluster-by-cluster growth takes place [12,33].

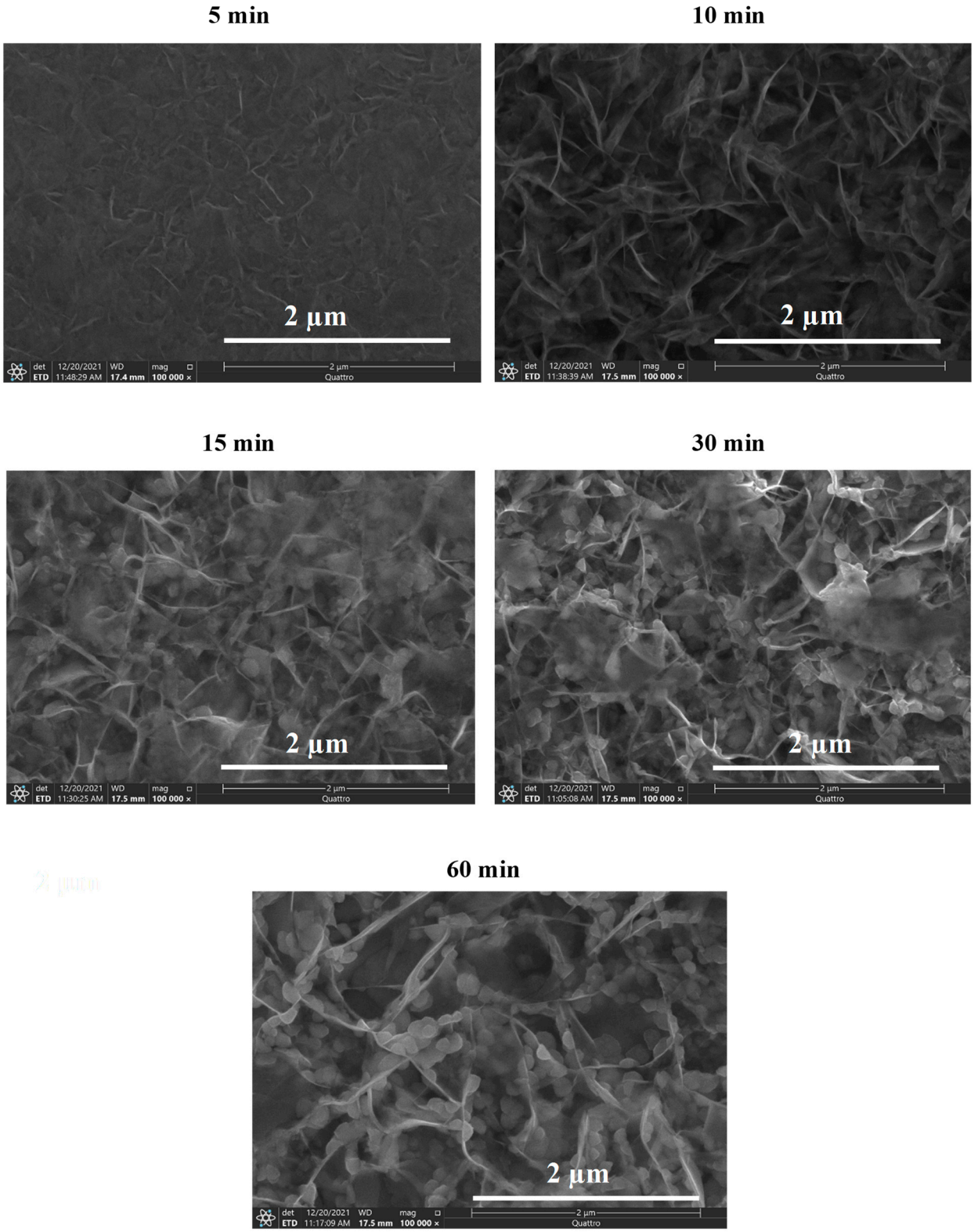

Figure 5. Top-view SEM images of CdS thin films at various deposition times.

Figure 6 demonstrates a cross-section view of SEM images for the fabricated CdS thin films at different deposition times. It is clear that the thin film thickness increases with increasing deposition time, where it has average values of about 0.073, 0.114, 0.625, 3, and 4.8 µm for deposition times of 5, 10, 15, 30, and 60 min, respectively. Moreover, the roughness is expected to increase with time, as presented for 5 and 10 min. This also could

be explained by different growth rates depending on the precursor concentrations where, at shorter times, ion-by-ion growth takes place; however, at longer times, cluster-by-cluster growth takes place [12,33]. Figure 7 shows EDX analysis for the samples where the ratio of Cd and S in the composite is extremely similar, which indicates the formation of the same phase of CdS thin films.

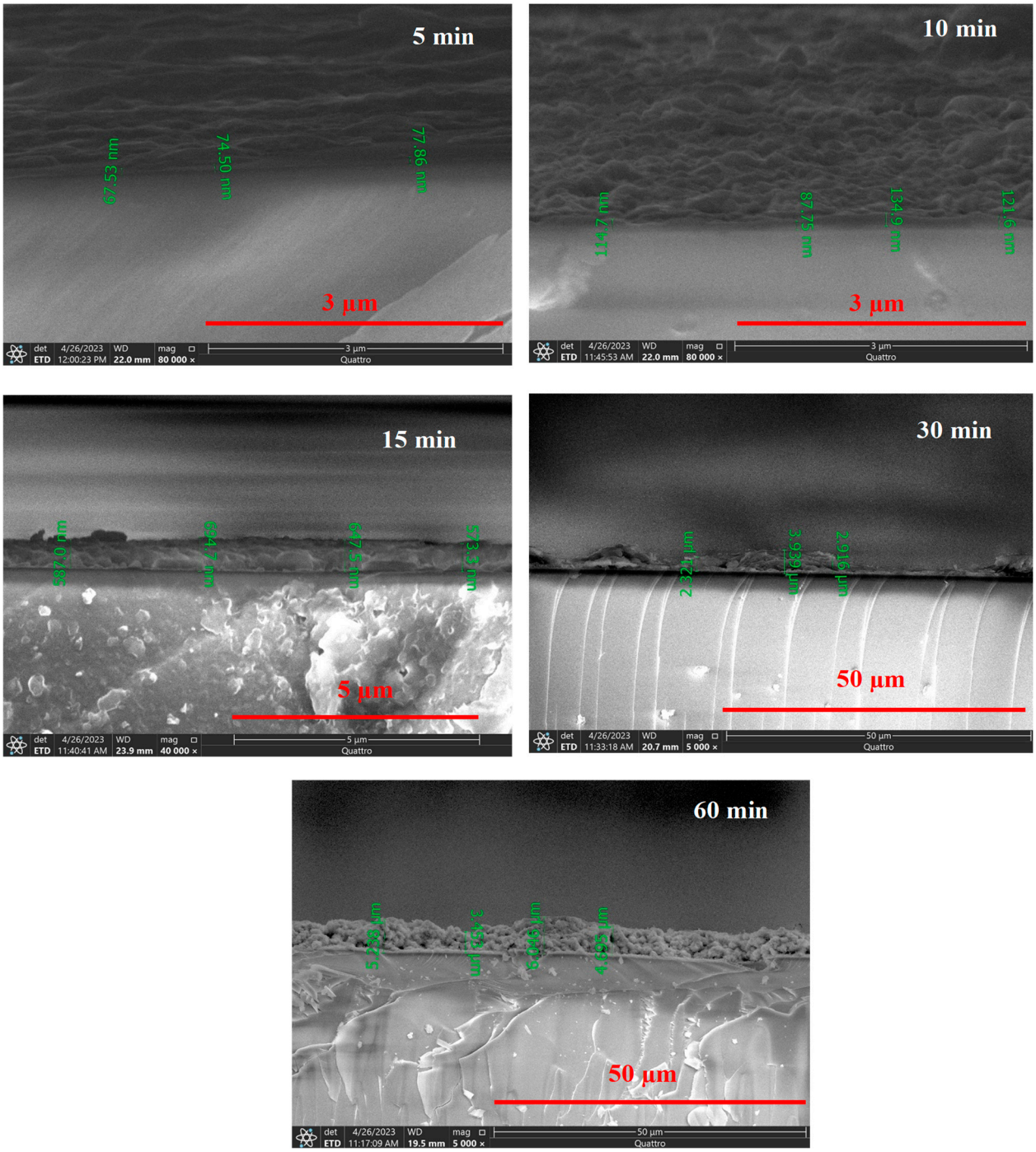

Figure 6. Cross-sectional SEM images of CdS thin films at various deposition times.

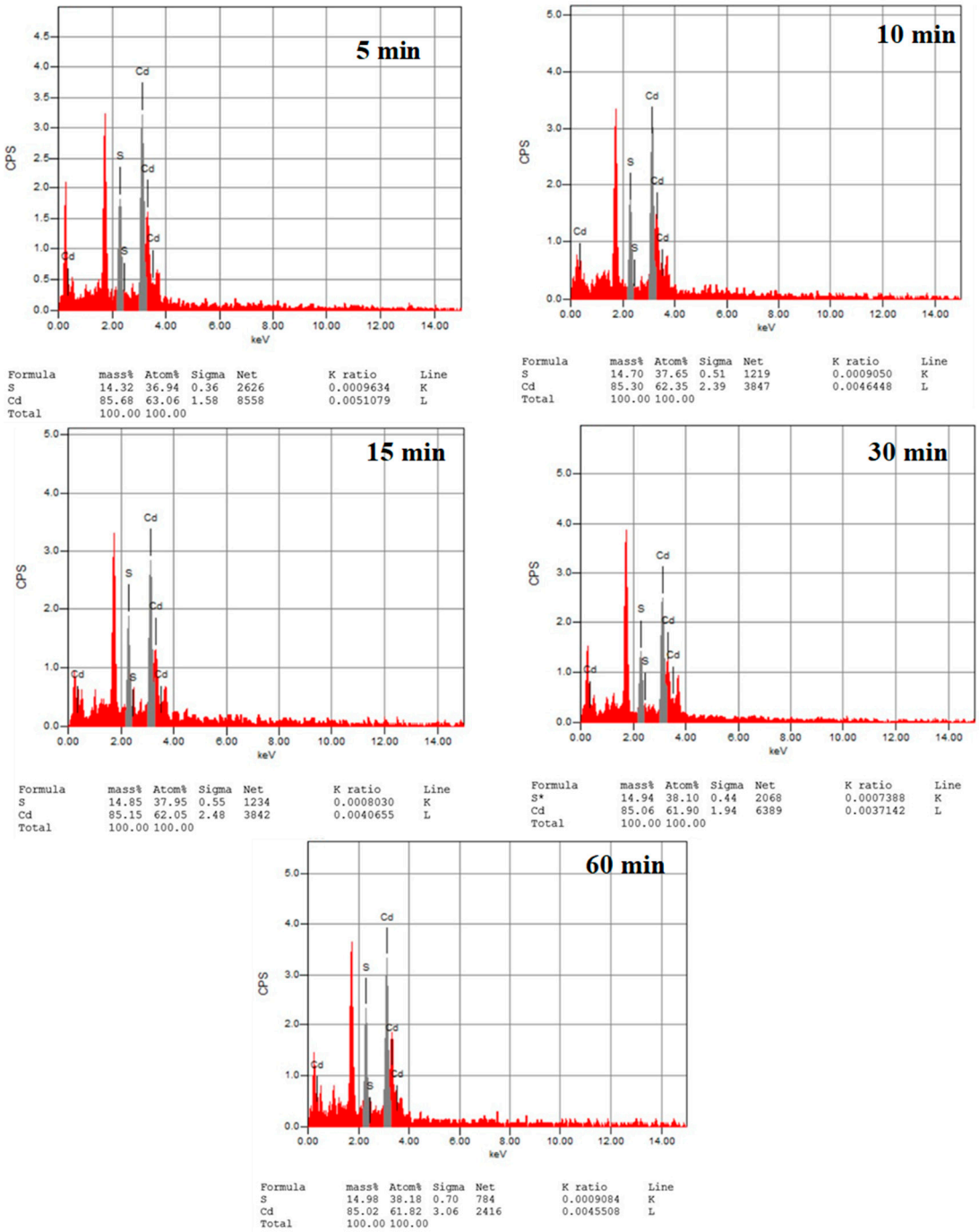

Figure 7. EDX analysis of CdS thin films at various deposition times (red color for glass substrates).

3.3. Raman Analysis

Raman spectroscopy is used to examine the lattice vibrations of generated thin films [13]. Figure 8 displays Raman spectra of CdS thin film at different deposition times. All fabricated thin films have two distinct peaks that are centered at 298 cm^{-1} and 599 cm^{-1}, indicating principal vibrations modes of CdS thin film. Each peak is the result of the longitudinal optical (1 LO and 2LO) phonons' first- and second-order scattering [14–16]. The ratio of 2LO/1LO intensity has commonly been used to measure the CdS crystallinity in samples [13]. It is significant to observe that, compared to longer deposition times, the 1LO Raman peak intensity is stronger at 5 min of deposition. The size of the crystallites, the effect of surface phonon mode, or the interface stress could all be contributing factors

to these differences in peak intensity [17]. This demonstrates the existence of the effect of surface optical phonon mode. The fluctuation in particle size is due to the variation in phonon momentum [18]. In comparison to bulk CdS, a Raman shift in the longitudinal optical phonon vibration frequency between 305–299 cm^{-1} and 610–599 cm^{-1} was observed, which agreed well with published results [9,15].

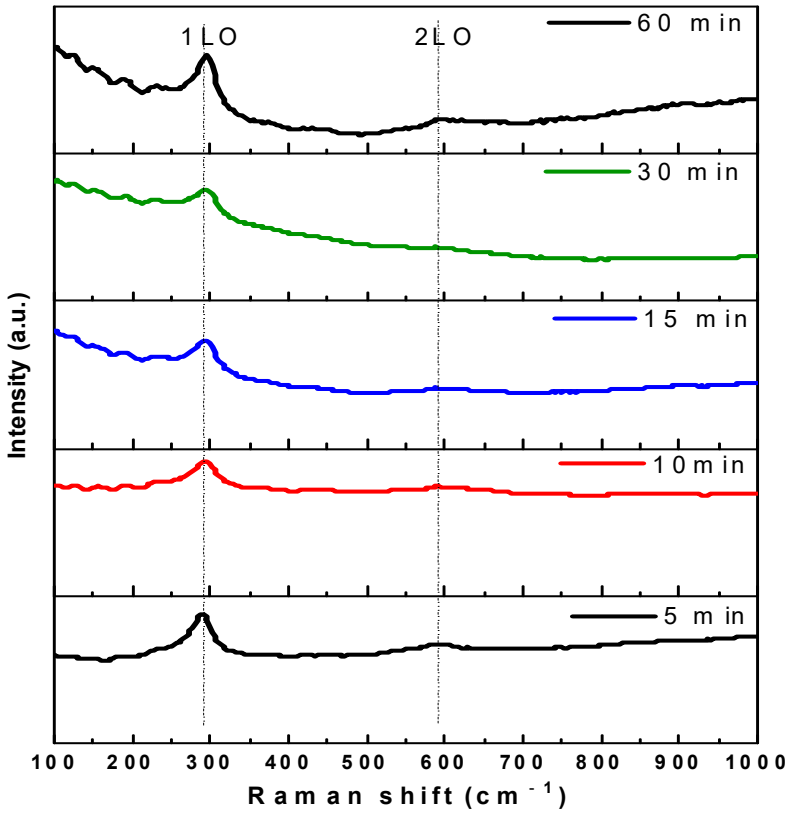

Figure 8. Raman spectra of CdS thin film at various deposition times.

3.4. Optical Properties

Figure 9 shows the UV-vis absorption spectra of the fabricated CdS thin films, where all samples have well-defined absorption band edges near 500 nm related to the band gap values of CdS thin films. The band gap energy (Eg) could be calculated from Tauc's relation, where the $(\alpha h\nu)^{n}$ versus hυ graph's intercept on the *X*-axis represents the linear region as presented in Figure 10 [19].

The Tauc relation to determine the band gap energy of a CdS thin film is given by

$$(\alpha h\nu)^{n} = A\left(h\nu - E_g\right) \quad (5)$$

where α is the absorption coefficient, A is a constant, h is Planck's constant, υ is the frequency, E_g is the band gap, and hν is the energy of the photon. For direct allowed and forbidden transitions, the value of superscript n varies between 2 or 2/3 and 1/2 or 1/3, respectively [5]. The primary absorption edge of Equation (5) exhibits the best linear fit for n = 2, which suggests that there are direct optical band gaps in the thin films. The estimated E_g of the CdS thin films is shown in Table 1, where it decreases with increasing deposition time, falling from 2.4 eV to 2.22 eV for samples deposited for 5 and 60 min. These E_g values were comparable to and well aligned with earlier experimental findings [21]. The lowest E_g value (2.21 eV), which was measured at 60 min, proves that crystallinity improved with increasing deposition time [9]. The CdS thin film thickness increases as the deposition period is prolonged; as a result, the band gap decrease [6] as well as the creation of allowed energy states produce a lower value of E_g, while small particles and grains

give a higher value [36]. Figure 11 shows the variation in E_g and nanoparticle crystallite size with changing CdS deposition time. The band gap energy increases with decreasing average crystallite size and rising molar concentration of parent samples because of the quantum confinement effect [23]. Therefore, the transmittance behavior of fabricated CdS thin films is improved in the visible range, and an energy gap of about 2.3 eV supports their suitability for use in solar cell applications.

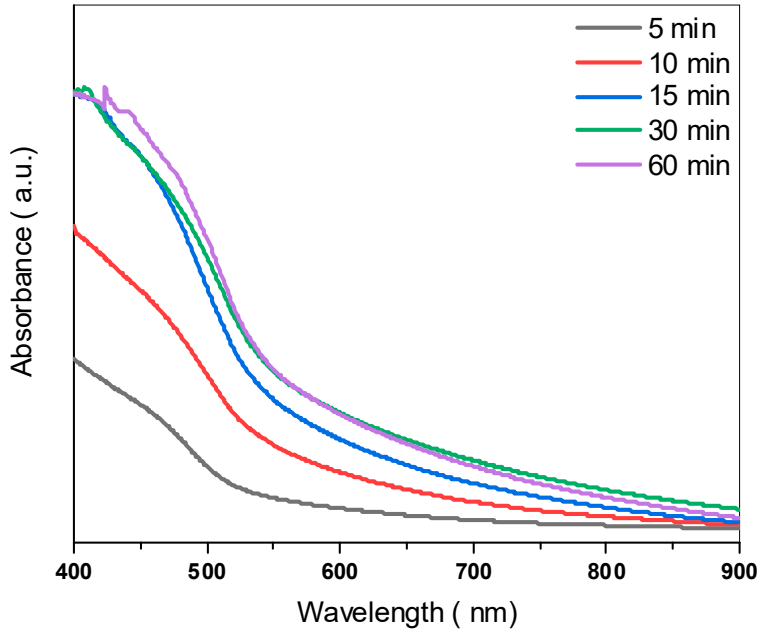

Figure 9. UV-Vis absorbance spectra of the fabricated CdS thin films.

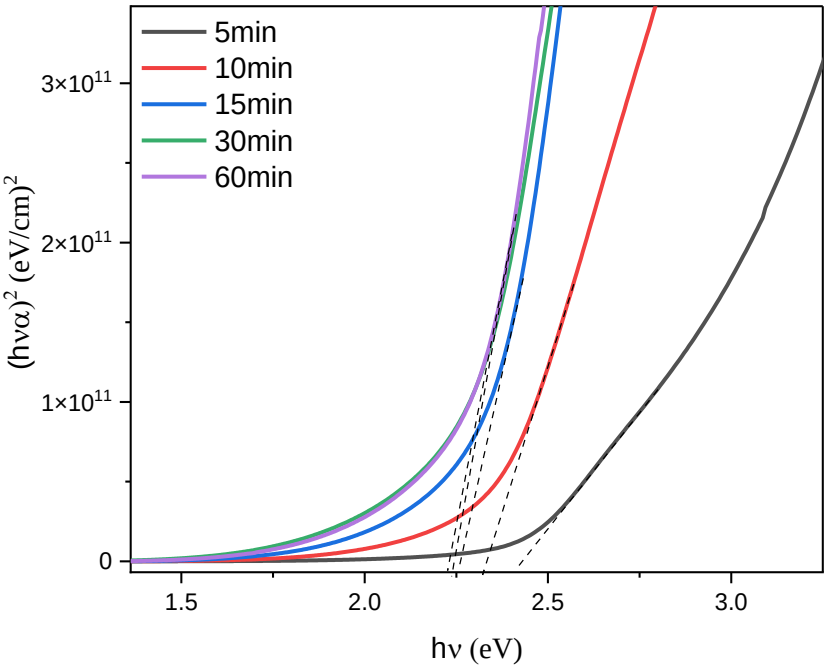

Figure 10. Tauc's plot of CdS thin films to estimate Eg values.

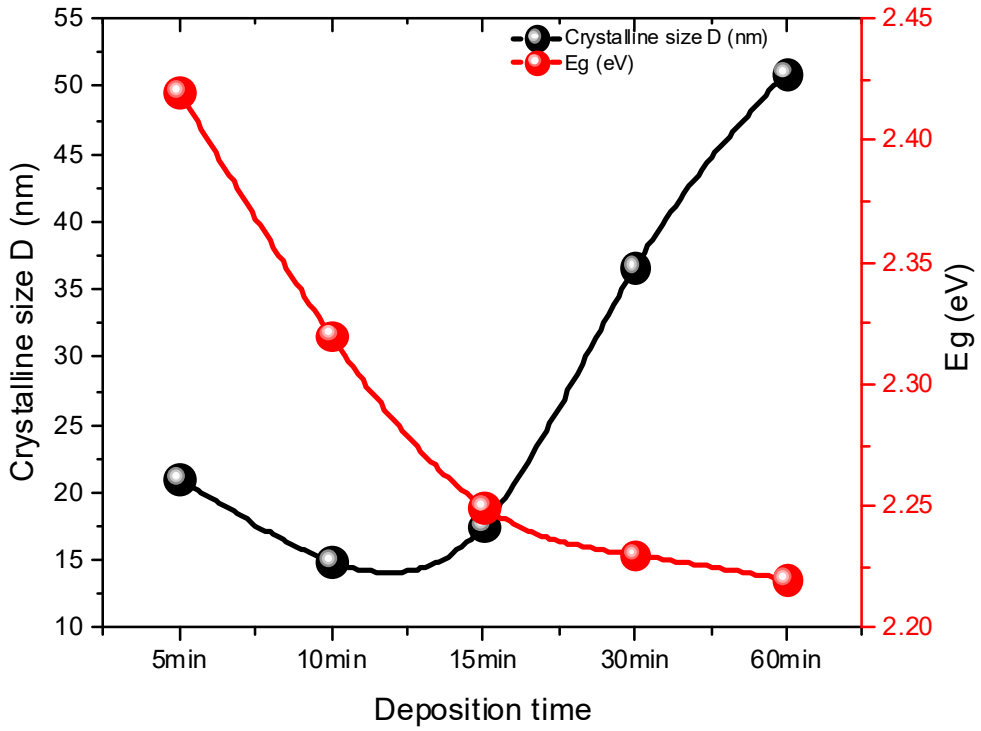

Figure 11. Variation of Eg and D of the fabricated CdS thin films with different deposition times.

3.5. PL Studies

Studies on photoluminescence (PL) provide important insights into atomic structure and material quality. PL spectra for CdS thin films were captured at ambient conditions, as presented in Figure 12. For PL emission and absorption spectra, flaws such as vacancies or electron-hole recombination sites were clearly present [24]. The main peaks appeared at 537 nm (2.30 eV) and at about 710 nm (1.75 eV) at room temperature. These could be attributed to the transition from the valence band to the conduction band and excitonic transitions (for example, pairs recombination and emissions where excitonic transitions are due to the cadmium interstitials (Cd) or sulfur vacancies (S) defects existing in CdS thin films) [37]. The near-band edge (NBE) emission from free excitons recombining causes the emission peak for all deposited CdS thin films at around 2.3 eV [25]. The optical band gap values measured almost exactly match the CdS thin film's emission peak position. Due to the Cd vacancies acting as acceptors (defects) or centers to capture carriers, which decrease as deposition time increases, photoluminescence declines as deposition time rises. Such defects decrease as the boundary between particles increases. The intensity decreases as deposition time increases, which suggests lesser carriers' recombination as well as higher separation and collection of charge carriers. Results show that CdS thin films are appropriate candidates for solar cells.

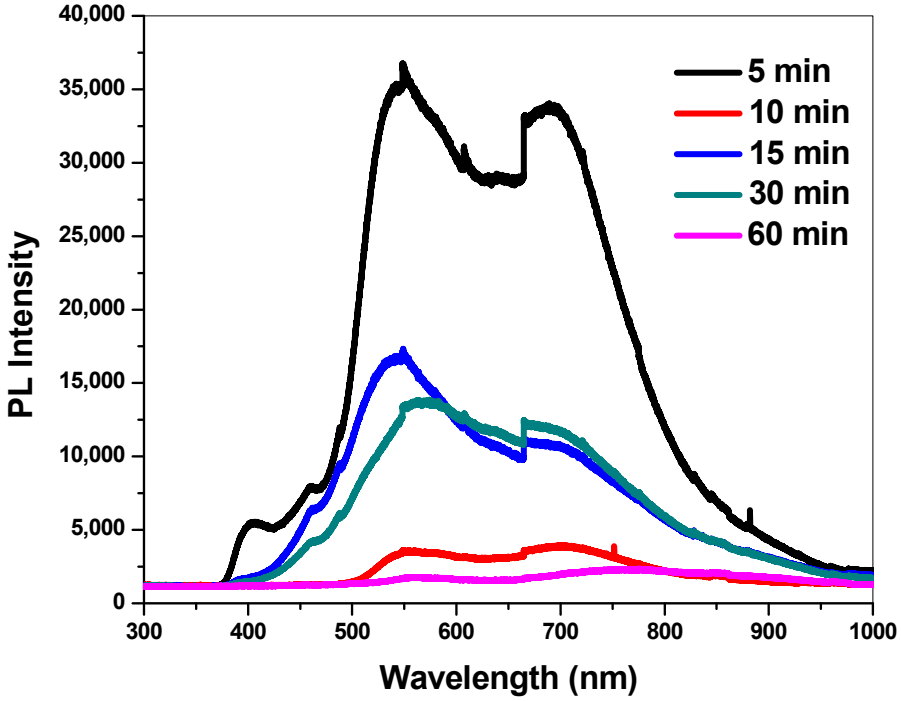

Figure 12. PL spectra for CdS thin films with different deposition times.

4. Conclusions

In summary, low-cost and low-temperature chemical bath deposition was employed successfully to fabricate CdS thin films. The structural, morphological, and optical properties of fabricated samples were characterized using different techniques. Polycrystalline cubic and hexagonal structures were formed for the fabricated CdS thin films with a uniformly thin film morphology that is flat and well-adhered to the substrate surface with hierarchical nanoflakes. Such a morphology could be a viable option to increase light absorption in the case of solar cell applications. Two characteristic vibration modes of CdS thin film appeared from Raman measurements. The thin films demonstrated strong absorption band edges near 500 nm, which are associated with band gap values of CdS. The predictable Eg for the fabricated CdS thin films was found to vary from 2.4 to 2.22 eV, which is a suitable value to enhance light absorption and generation for optoelectronic devices. PL results indicate the formation of CdS thin films where two peaks appeared at 537 nm and about 710 nm and intensity decreased as deposition time increased, which suggest lesser carriers' recombination as well as higher separation and collection of charge carriers. Our outcomes reveal that CdS thin films are suitable candidates for optoelectronic applications, especially solar cells.

Supplementary Materials: The following supporting information can be downloaded at: https://www.mdpi.com/article/10.3390/cryst13050788/s1.

Author Contributions: Conceptualization, A.E.-S. and S.E.; methodology, A.E.-S., S.E., T.M.M. and S.A.E.-A.; validation, A.E.-S., M.A.H., T.M.M. and S.A.E.-A.; formal analysis, S.E. and A.E.-S.; investigation, A.E.-S., S.E., T.M.M. and S.A.E.-A.; resources, S.E. and M.A.H.; data curation; T.M.M. and S.A.E.-A.; writing—original draft preparation, A.E.-S., S.E., M.A.H., T.M.M. and S.A.E.-A.; writing—review and editing S.E., O.K.A., A.E.-S., T.M.M. and S.A.E.-A.; visualization, M.A.H.; supervision, A.E.-S., T.M.M. and S.A.E.-A.; project administration A.E.-S., T.M.M. and S.A.E.-A.; funding acquisition, M.A.H. and O.K.A. All authors have read and agreed to the published version of the manuscript.

Funding: The authors extend their appreciation to the Deanship of Scientific Research at Imam Mohammad Ibn Saud Islamic University for funding this work through Research Group no. RG-21-09-82.

Data Availability Statement: Data available on request.

Conflicts of Interest: The manuscript was written through the contributions of all authors. All authors have given approval to the final version of the manuscript. The authors declare no competing financial interest.

References

1. Ashok, A.; Regmi, G.; Romero-Núñez, A.; Solis-López, M.; Velumani, S.; Castaneda, H. Comparative studies of CdS thin films by chemical bath deposition techniques as a buffer layer for solar cell applications. *J. Mater. Sci. Mater. Electron.* **2020**, *31*, 7499–7518. [CrossRef]
2. Abou-Ras, D.; Kostorz, G.; Romeo, A.; Rudmann, D.; Tiwari, A. Structural and chemical investigations of CBD-and PVD-CdS buffer layers and interfaces in Cu (In, Ga) Se_2-based thin film solar cells. *Thin Solid Film.* **2005**, *480*, 118–123. [CrossRef]
3. Rahman, M.; Hossain, J.; Kuddus, A.; Tabassum, S.; Rubel, M.H.; Shirai, H.; Ismail, A.B.M. A novel synthesis and characterization of transparent CdS thin films for CdTe/CdS solar cells. *Appl. Phys. A* **2020**, *126*, 145. [CrossRef]
4. Lokhande, C.; Ennaoui, A.; Patil, P.; Giersig, M.; Muller, M.; Diesner, K.; Tributsch, H. Process and characterisation of chemical bath deposited manganese sulphide (MnS) thin films. *Thin Solid Film.* **1998**, *330*, 70–75. [CrossRef]
5. Sinha, T.; Lilhare, D.; Khare, A. Temperature-dependent structural, morphological and optical properties of chemical bath-deposited CdS films. *Rare Met.* **2021**, *40*, 701–707. [CrossRef]
6. Ichimura, M.; Goto, F.; Arai, E. Structural and optical characterization of CdS films grown by photochemical deposition. *J. Appl. Phys.* **1999**, *85*, 7411–7417. [CrossRef]
7. Sathish, M.; Viswanath, R. Photocatalytic generation of hydrogen over mesoporous CdS nanoparticle: Effect of particle size. noble metal and support. *Catal. Today* **2007**, *129*, 421–427. [CrossRef]
8. Ouachtari, F.; Rmili, A.; Elidrissi, B.; Bouaoud, A.; Erguig, H.; Elies, P. Influence of bath temperature, deposition time and S/Cd ratio on the structure, surface morphology, chemical composition and optical properties of CdS thin films elaborated by chemical bath deposition. *J. Mod. Phys.* **2011**, *2011*, 1073–1082. [CrossRef]
9. Kumar, A.; Pednekar, D.; Mukherjee, S.; Choubey, R.K. Effect of deposition time and complexing agents on hierarchical nanoflake-structured CdS thin films. *J. Mater. Sci. Mater. Electron.* **2020**, *31*, 17055–17066. [CrossRef]
10. Abdelfatah, M.; Salah, H.Y.; El-Henawey, M.I.; Oraby, A.H.; El-Shaer, A.; Ismail, W. Insight into Co concentrations effect on the structural, optical, and photoelectrochemical properties of ZnO rod arrays for optoelectronic applications. *J. Alloys Compd.* **2021**, *873*, 159875. [CrossRef]
11. Salah, H.; Mahmoud, K.; Ismail, W.; El-Shaer, A.; Oraby, A.; Abdelfatah, M.; EL-Henawey, M. Influence of Nickel Concentration on the Microstructure, Optical, Electrical, and Photoelectrochemical Properties of ZnO Nanorods Synthesized by Hydrothermal Method. *J. Electron. Mater.* **2022**, *51*, 910–920. [CrossRef]
12. Salem, S.M.; Deraz, N.M.; Saleh, H.A. Fabrication and characterization of chemically deposited copper–manganese sulfide thin films. *Appl. Phys. A* **2020**, *126*, 700. [CrossRef]
13. Kwon, J.-H.; Ahn, J.-S.; Yang, H. Chemical bath deposition of CdS channel layer for fabrication of low temperature-processed thin-film-transistors. *Curr. Appl. Phys.* **2013**, *13*, 84–89. [CrossRef]
14. Lee, J. Raman scattering and photoluminescence analysis of B-doped CdS thin films. *Thin Solid Film.* **2004**, *451*, 170–174. [CrossRef]
15. Shen, X.-P.; Yuan, A.-H.; Wang, F.; Hong, J.-M.; Xu, Z. Fabrication of well-aligned CdS nanotubes by CVD-template method. *Solid State Commun.* **2005**, *133*, 19–22. [CrossRef]
16. Khan, Z.; Shkir, M.; Ganesh, V.; AlFaify, S.; Yahia, I.; Zahran, H. Linear and nonlinear optics of CBD grown nanocrystalline F doped CdS thin films for optoelectronic applications: An effect of thickness. *J. Electron. Mater.* **2018**, *47*, 5386–5395. [CrossRef]
17. Rondiya, S.; Rokade, A.; Gabhale, B.; Pandharkar, S.; Chaudhari, M.; Date, A.; Chaudhary, M.; Pathan, H.; Jadkar, S. Effect of bath temperature on optical and morphology properties of CdS thin films grown by chemical bath deposition. *Energy Procedia* **2017**, *110*, 202–209. [CrossRef]
18. Khan, Z.R.; Shkir, M.; Alshammari, A.S.; Ganesh, V.; AlFaify, S.; Gandouzi, M. Structural, linear and third order nonlinear optical properties of sol-gel grown Ag-CdS nanocrystalline thin films. *J. Electron. Mater.* **2019**, *48*, 1122–1132. [CrossRef]
19. Tauc, J. *Optical Properties of Solids 22*; Abeles, F., Ed.; North Holland Pub: Amsterdam, The Netherlands, 1970.
20. Abel, S.; Tesfaye, J.L.; Gudata, L.; Lamessa, F.; Shanmugam, R.; Dwarampudi, L.P.; Nagaprasad, N.; Krishnaraj, R. Investigating the Influence of Bath Temperature on the Chemical Bath Deposition of Nanosynthesized Lead Selenide Thin Films for Photovoltaic Application. *J. Nanomater.* **2022**, *2022*, 3108506. [CrossRef]
21. Priya, N.S.; Kamala, S.S.P.; Anbarasu, V.; Azhagan, S.A.; Saravanakumar, R. Characterization of CdS thin films and nanoparticles by a simple chemical bath technique. *Mater. Lett.* **2018**, *220*, 161–164. [CrossRef]
22. Khot, K.V.; Mali, S.S.; Pawar, N.B.; Kharade, R.R.; Mane, R.M.; Kondalkar, V.V.; Patil, P.B.; Patil, P.S.; Hong, C.K.; Kim, J.H. Development of nanocoral-like Cd (SSe) thin films using an arrested precipitation technique and their application. *New J. Chem.* **2014**, *38*, 5964–5974. [CrossRef]
23. Ghazi, M.; Izadifard, M.; Ghodsi, F.E.; Yuonesi, M. Studying Mn-and Ni-doped ZnO thin films synthesized by the sol–gel method. *J. Supercond. Nov. Magn.* **2012**, *25*, 101–108. [CrossRef]
24. Mazón-Montijo, D.A.; Sotelo-Lerma, M.; Quevedo-López, M.; El-Bouanani, M.; Alshareef, H.N.; Espinoza-Beltrán, F.J.; Ramírez-Bon, R. Morphological and chemical study of the initial growth of CdS thin films deposited using an ammonia-free chemical process. *Appl. Surf. Sci.* **2007**, *254*, 499–505. [CrossRef]

25. Oliva, A.I.; Rodríguez, R.C.; Ceh, O.; Pérez, P.B.; Briones, F.C.; Sosa, V. First stages of growth of CdS films on different substrates. *Appl. Surf. Sci.* **1999**, *148*, 42–49. [CrossRef]
26. Kozhevnikova, N.S.; Vorokh, A.S.; Uritskaya, A.A. Cadmium sulfide nanoparticles prepared by chemical bath deposition. *Russ. Chem. Rev.* **2015**, *84*, 225. [CrossRef]
27. Manjakkal, L.; Szwagierczak, D.; Dahiya, R. Metal oxides based electrochemical pH sensors: Current progress and future perspectives. *Prog. Mater. Sci.* **2020**, *109*, 100635. [CrossRef]
28. Abdelfatah, M.; Ismail, W.; El-Shafai, N.M.; El-Shaer, A. Effect of thickness, bandgap, and carrier concentration on the basic parameters of Cu_2O nanostructures photovoltaics: Numerical simulation study. *Mater. Technol.* **2021**, *36*, 712–720. [CrossRef]
29. Abdelfatah, M.; El-Shaer, A. One step to fabricate vertical submicron ZnO rod arrays by hydrothermal method without seed layer for optoelectronic devices. *Mater. Lett.* **2018**, *210*, 366–369. [CrossRef]
30. Ismail, W.; El-Shafai, N.M.; El-Shaer, A.; Abdelfatah, M. Impact of substrate type on the surface and properties of electrodeposited Cu_2O nanostructure films as an absorber layer for solar cell applications. *Mater. Sci. Semicond. Process.* **2020**, *120*, 105335. [CrossRef]
31. Moualkia, H.; Hariech, S.; Aida, M.S. Structural and optical properties of CdS thin films grown by chemical bath deposition. *Thin Solid Film.* **2009**, *518*, 1259–1262. [CrossRef]
32. Barote, M.A.; Yadav, A.A.; Masumdar, E.U. Synthesis, characterization and photoelectrochemical properties of n-CdS thin films. *Phys. B Condens. Matter* **2011**, *406*, 1865–1871. [CrossRef]
33. Sandoval-Paz, M.G.; Ramírez-Bon, R. Analysis of the early growth mechanisms during the chemical deposition of CdS thin films by spectroscopic ellipsometry. *Thin Solid Film.* **2009**, *517*, 6747–6752. [CrossRef]
34. Najm, A.S.; Naeem, H.S.; Majdi, H.S.; Hasbullah, S.A.; Hasan, H.A.; Sopian, K.; Bais, B.; Al-Iessa, H.J.; Dhahad, H.A.; Ali, J.M.; et al. An in-depth analysis of nucleation and growth mechanism of CdS thin film synthesized by chemical bath deposition (CBD) technique. *Sci. Rep.* **2022**, *12*, 15295. [CrossRef] [PubMed]
35. Maghouli, M.; Eshghi, H. Effect of deposition time on physical properties of nanostructured CdS thin films grown by chemical bath deposition technique. *Superlattices Microstruct.* **2019**, *128*, 327–333. [CrossRef]
36. Islam, S.; Hossain, T.; Sarwar, H.; Rashid, M.J. A systematic study on chemically deposited cadmium sulfide (CdS) thin film. *J. Theor. Appl. Phys.* **2020**, *14*, 265–274. [CrossRef]
37. Hariech, S.; Bougdira, J.; Belmahi, M.; Medjahdi, G.; Aida, M.S.; Zertal, A. Effect of deposition time on chemical bath deposited CdS thin films properties. *Bull. Mater. Sci.* **2022**, *45*, 78. [CrossRef]